Massive disturbance of the daytime lower ionosphere by the giant γ-ray flare from magnetar SGR 1806−20

U. S. Inan,[1] N. G. Lehtinen,[1] R. C. Moore,[1] K. Hurley,[2] S. Boggs,[2] D. M. Smith,[3] and G. J. Fishman[4]

[1] The giant γ-ray flare from SGR 1806-20 created a massive disturbance in the daytime lower ionosphere, as evidenced by unusually large changes in amplitude/phase of subionospherically propagating VLF signals. The perturbations of the 21.4 kHz NPM (Lualualei, Hawaii) signal observed at PA (Palmer Station, Antarctica) correspond to electron densities increasing by a factor of ~100 to $\sim10^3$ cm^{-3} at ~60 km and $\gtrsim1000$ to ~10 cm^{-3} at ~30 km altitude. Enhanced conductivity produced by flare onset endured for >1 hour, the time scale determined by mutual neutralization. A brief (~100 ms) low frequency (~3 to 6 kHz) emission is also observed during the flare onset. **Citation:** Inan, U. S., N. G. Lehtinen, R. C. Moore, K. Hurley, S. Boggs, D. M. Smith, and G. J. Fishman (2007), Massive disturbance of the daytime lower ionosphere by the giant γ-ray flare from magnetar SGR 1806−20, *Geophys. Res. Lett.*, *34*, L08103, doi:10.1029/2006GL029145.

1. Introduction

[2] VLF remote sensing is a sensitive technique to detect transient disturbances of the nighttime lower ionosphere (~40 to 90 km altitude), resulting from high energy auroral precipitation [e.g., *Potemra and Rosenbert*, 1973; *Cummer et al.*, 1997], lightning-induced electron precipitation [e.g., *Inan and Carpenter 1987*], electromagnetic and quasi-electrostatic coupling produced by lightning discharges (e.g., sprites and elves) [*Inan et al.*, 1996; *Moore et al.*, 2003; *Haldoupis et al.*, 2004; *Cheng and Cummer*, 2005], cosmic gamma-ray bursts (GRBs) [*Fishman and Inan*, 1988], and γ-ray flares from a magnetar [*Inan et al.*, 1999]. VLF detection of daytime ionospheric disturbances is less common, but include solar X-ray flares [*Mitra*, 1974].

[3] On December 27, 2004, at $\sim$21:30:26.5 UT (mid-day in Central Pacific), a giant (in intensity) hard X-ray/γ−ray flare, near the solar zenith, substantially ionized the exposed part of Earth's day-side ionosphere. The flare originated from magnetar SGR 1806−20 at 12−15 kpc from Earth [*Hurley et al.*, 2005], with sub-solar point 146.2°W 20.4°S, i.e., middle of Pacific Ocean. The burst arrived nearly at local noon, on the dayside ionosphere. The γ-ray fluence was $\sim10^3$ times larger than SGR 1900 + 14 [e.g., *Inan et al.*

1999]. The intense onset of the flare lasted for ~600 ms with a peak flux of ~20 erg cm^{-2} s^{-1} and a total fluence of ~2 erg cm^{-2} [*Terasawa et al.*, 2005]. The initial peak was followed by an oscillating tail (7.56 s period) persisting for ~380 s [*Hurley et al.*, 2005], with a fluence of only $\sim0.3\%$ of the total. An afterglow [*Mereghetti et al.*, 2005], lasted for ~6000 s, with a flux $\sim10^6$ times less than onset and with a fluence same as the oscillating tail. A composite of the γ-ray data reported by GEOTAIL [*Terasawa et al.*, 2005], RHESSI [*Hurley et al.*, 2005], and INTEGRAL [*Mereghetti et al.*, 2005] spacecraft is plotted in Figure 1.

[4] The γ-ray flare massively disturbed the daytime lower ionosphere down to ~20 km altitude for >1 hour, substantially extending the altitudinal range affected by an extra-solar object. The >1 hour duration of VLF perturbations implies persistence of ionospheric disturbance well beyond the intense flare onset and even the afterglow. A detailed analysis of VLF signatures measured at PA (Palmer) reveals that the perturbation is dominated solely by the initial intense γ-ray onset, and that the hour-long recovery is due to the ion mutual neutralization rate at altitudes <60 km.

2. Observations

[5] The amplitude/phase of NPM signal at PA (the entire >12 Mm path illuminated by γ-ray flare) show an immediate (<20 ms) onset and an initial quick (<500 ms) recovery, followed by a long-duration (>1 hour) recovery (Figure 2). Signals at PA received from other VLF transmitters NAA (24.0 kHz, Cutler, ME) and NLK (24.8 kHz, Jim Creek, WA) are similarly perturbed (not shown), but the better defined NPM signal is used from here on. The NPM-PA signal has been extensively studied for nighttime ionospheric disturbances [e.g., *Lev-Tov et al.*, 1996; *Inan et al.*, 1999], and is well suited due to its single-waveguide-mode content, as an all-sea-based and mid-to-low latitude VLF path [*Inan and Carpenter*, 1987].

[6] The sudden VLF onset (<20 ms) is coincident with RHESSI flare onset. The maximum VLF amplitude and phase deviations of 26.5 dB and 328° are reached within ~200 ms of flare onset, when RHESSI detectors stopped counting due to saturation. These unprecedented daytime changes suggest substantial lowering of VLF reflection height. Similar perturbations were readily detectable in narrowband VLF data at other sites (e.g., University of Louisville, KY, available at http://moondog.astro.louisville.edu/).

[7] Event onset is followed by an unusually quick (<500 ms) exponential recovery to signal amplitude/phase levels of ~8 dB and $\sim120°$, indicating a high X-ray content of the initial spike producing ionization at altitudes $\lesssim60$ km, where recovery rates (for enhanced ionization) are <1 s.

¹Space, Telecommunications, and Radioscience Laboratory, Electrical Engineering Department, Stanford University, Stanford, California, USA.
²Space Sciences Laboratory, University of California, Berkeley, California, USA.
³Department of Physics, University of California, Santa Cruz, California, USA.
⁴NASA Marshall Space Flight Center, Huntsville, Alabama, USA.
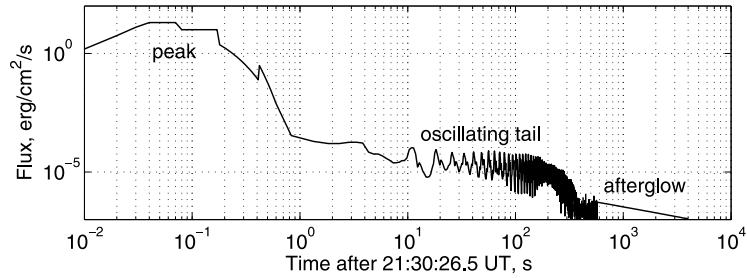
Figure 1. The γ-ray flux versus time, showing the peak [*Terasawa et al.*, 2005], oscillating tail [*Hurley et al.*, 2005] and the afterglow ($\propto t^{-0.85}$ [*Mereghetti et al.*, 2005]).

[8] Starting ~400 ms after onset, RHESSI detector data show that the flare lasted for ~380 s, decreasing in intensity and exhibiting a ~7.56 s modulation. The NPM-PA amplitude/phase continue to recover, rather than further decrease in amplitude or advance in phase, indica-ting that ionization by the initial spike was much larger than that due to the rest of the flare (Figure 2b). The ~7.56 s modulation was not detectable in VLF data (Figure 2b), upon Fourier analysis, in contrast to the detection of pulsation from SGR 1900+14 [*Inan et al.*, 1999].
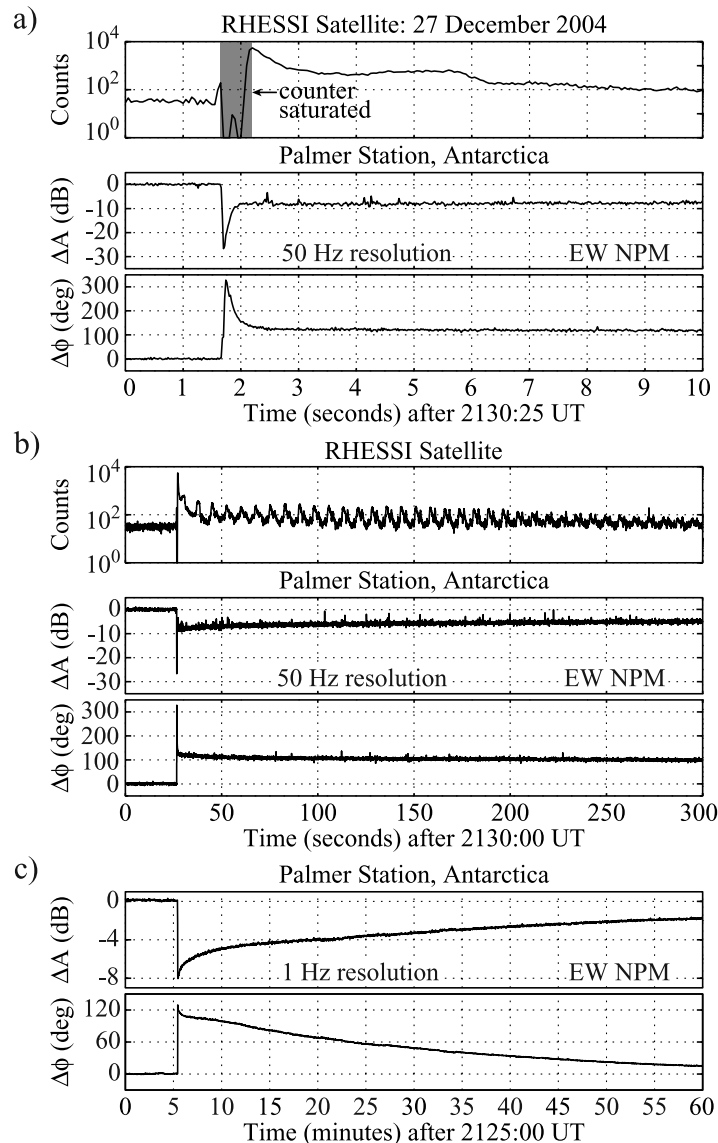
Figure 2. RHESSI and narrowband VLF observations: (a) 10 s after the flash; (b) 5 min after the flash; (c) ~1 h after the flash.
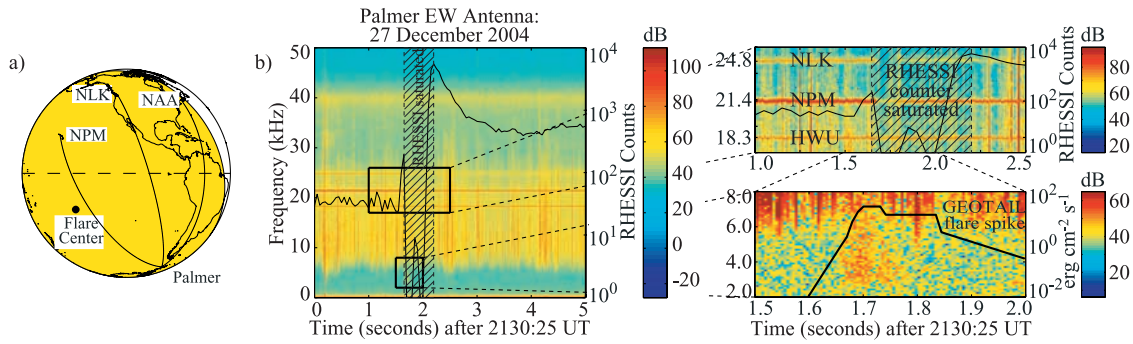
Figure 3. (a) VLF paths to Palmer; area illuminated by γ-flare. (b) Emission at 2–6 kHz during the flare spike, with superimposed RHESSI and GEOTAIL data.

[9] At the time of apparent flare termination on RHESSI, i.e., at $\sim$450 s after the onset, the VLF amplitude/phase are still $\sim$4.5 dB and $\sim$90° (Figure 2c). Recovery of VLF perturbation continues for >1 hour, much longer than characteristic recovery times at altitudes below daytime VLF reflection height of $\sim$70 km. This extended signature is not due to flare afterglow [*Mereghetti et al.*, 2005], since its intensity is even lower than the non-detectable oscillating part.

[10] The effect of this γ-ray flare is also evident in broadband VLF data. The narrowband transmitters (horizontal lines) in Figure 3 disappear briefly, and even lightning-induced sferics (vertical lines) tend to decrease in amplitude during the event. The lower-right panel shows a mysterious enhanced emission in 3–6 kHz range during the flare onset, lasting for $\lesssim$100 ms, and corresponding to the initial flare peak, which could be a direct effect of the γ-ray flare or a modification of the Earth-ionosphere waveguide. However, the former is more likely since lowering of reflection height would increase the cutoff frequency for waveguide modes. This emission may be similar to electromagnetic pulse (EMP) produced in nuclear tests [*Karzas and Latter*, 1965]. However, the nuclear EMP is impulsive due to very short ($\sim\mu$s) duration of γ-ray emission, while this emission appears as incoherent burst of noise. Nevertheless, such an emission may be caused by the hydromagnetic exclusion of (and the subsequent repopulation by) the Earth's field in the volume within which ionization is produced by the flare, much like that which occurs for nuclear explosions [*Karzas and Latter*, 1962]. Although VLF emissions from nuclear explosions have been detected [*Allcock et al.*, 1963], quantitative assessment of the possibility of the same physical process being active here is beyond our scope.

3. Analysis

[11] The Monte Carlo model described by *Inan et al.* [1999] is used to calculate energy deposition and ionization by incident γ-rays, including Compton scattering and photoelectric absorption. Compton and photo electrons deposit their energy within 1 km, producing one electron-ion pair per 35 eV.

[12] Based on incident photon spectra from RHESSI and WIND, Monte Carlo photons were initially distributed by the black-body spectrum $f(\mathcal{E}) = C\mathcal{E}^2/(e^{\mathcal{E}/T} - 1)$ with $T = 175$ keV during the spike (the first 0.3 s) and optically thin thermal bremsstrahlung function $f(\mathcal{E}) = Ce^{-\mathcal{E}/T}/\mathcal{E}$ with $T = $ 22 keV during the oscillating part [*Hurley et al.*, 2005], for $\mathcal{E} = 0.2$ keV to 25 MeV. The afterglow flux is too low to produce detectable effects and is not modeled. Photons are propagated starting at altitude of 200 km, at various starting nadir angles ψ.

[13] Time evolution of electron and ion densities from 20 to 120 km altitude is calculated using a five-constituent model, an extension of *Glukhov et al.*'s [1992] model to be applicable at altitudes <50 km [*Lehtinen and Inan*, 2007]. Electrons (N_e), negative ions (N^-), light positive ions (N^+), positive ion clusters (N_x^+) and heavy negative ions (N_x^-) have densities described by:

$$\frac{dN_e}{dt} = Q - \beta_e N_e + \gamma_e N^- + \gamma_x N_x^- - (\alpha_d N^+ + \alpha_d^c N_x^+)N_e \quad (1)$$

$$\frac{dN^-}{dt} = \beta_e N_e - \gamma_e N^- \alpha_i (N^+ + N_x^+)N^- - AN^- \quad (2)$$

$$\frac{dN_x^-}{dt} = -\gamma_x N_x^- - \alpha_i (N^+ + N_x^+)N_x^- + AN^- \quad (3)$$

$$\frac{dN^+}{dt} = Q - \alpha_d N_e N^+ - \alpha_i (N^- + N_x^-)N^+ - BN^+ \quad (4)$$

$$\frac{dN_x^+}{dt} = -\alpha_d^c N_e N_x^+ - \alpha_i (N^- + N_x^-)N_x^+ + BN^+ \quad (5)$$

where mutual neutralization coefficient $\alpha_i \approx (10^{-7} + 10^{-24}N)$ cm^3 s^{-1}; dissociative recombination coefficients $\alpha_d = 6 \times 10^{-7}$ cm^3 s^{-1} and $\alpha_d = 10^{-5}$ cm^3 s^{-1}; attachment rate $\beta_e = 6 \times 10^{-32}N^2$; detachment rate $\gamma_e = (8.6 \times 10^{-10}e^{-\frac{6000}{T}}N + 2.5 \times 10^{-10}N_{ac} + 0.44)$ s^{-1}, with T being the neutral temperature, and the density of "active species" $N_{ac} = N[O] + N[N] + N[O_2(a^1\Delta_g)]$; rate of conversion of N^+ into N_x^+, $B = 10^{-31}N^2$ s^{-1}; photodetachment rate from heavy negative ions $\gamma_x = 0.002$ s^{-1}; rate of conversion of N^- into N_x^-, A (value discussed below); and N denotes the neutral molecule density. Q includes flare and ambient ionization sources. The flare energy is deposited mostly <30 km, with profile $\propto N$, due to deep penetration of high energy photons. Q is approximately $\propto$ total photon energy flux.
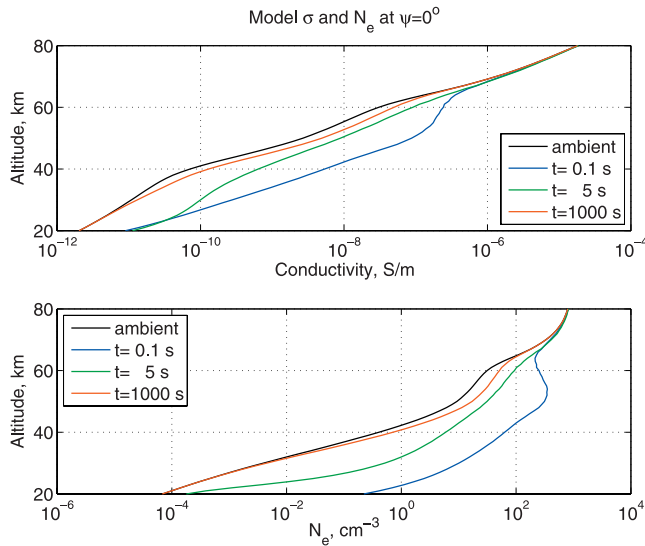
Figure 4. Conductivity (parallel) at different times for $\psi = 0°$, for low A and $N_{ac} = 0$.

[14] Conductivity (σ) and N_e profiles at three different times for $\psi = 0°$ are plotted in Figure 4. The change $\Delta\sigma$ depends on ψ insignificantly for $\psi \lesssim 60°$, with higher $\Delta\sigma$ produced at higher altitudes for $\psi > 60°$. $\Delta\sigma$ is due to changes in both electron and ion densities. For ~5 s, enhanced N_e levels render electron conductivity dominant even at <60 km, where ion conductivity dominates for ambient conditions. As ionization relaxes, electrons attach to background molecules, and ion conductivity is again dominant. Significant ionization and $\Delta\sigma$ persist for >1000 s, in agreement with observations (Figure 2).

[15] To compare calculated ionization profiles to VLF data, we use a numerical model of VLF propagation in Earth-ionosphere waveguide [*Lev-Tov et al.*, 1996, and references therein] to determine NPM–PA amplitude/phase at different times. The model describes electromagnetic field as sum of coupled waveguide modes, accounting for mode excitation factors at the source, imperfect conductance and curvature of ground/sea surfaces, arbitrary orientation of geomagnetic field, and effects of both ions and electrons. The model input is altitude profile of N_e (and thus σ) calculated using Monte Carlo model at different points along the path as function of corresponding ψ and time.

[16] Model results are presented in Figure 5, with different curves for variations of some of the five-species model parameters, namely negative ion conversion rate A and density of active species N_{ac}, which determines detachment rate γ_e. Rate A is determined by reactions of light negative ions such as CO_3^- and its hydrates with minor nitrogen-containing constituents, resulting in production of NO_3^- and its hydrates. Two relevant reactions are (1) with N_2O_5 or NO_2 at rate $\sim 2 \times 10^{-10} - 3 \times 10^{-10}$ cm^3 s^{-1} [*Fehsenfeld and Ferguson*, 1974; *Ferguson*, 1979]; (2) with NO at rate $\sim 1 \times 10^{-11}$ cm^3 s^{-1} [*Fehsenfeld and Ferguson*, 1974]. Relative importance of these reactions depends on abundances of minor constituents. Model results are examined for (1) a high value of A based on the first reaction and assuming $N[NO_2] \simeq N[N_2O]$, taken from *Jursa* [1985, p. 21–18], and (2) a low value (~100 times smaller) of A determined by the second reaction, which is the case when $N[NO] \simeq 0.2N[N_2O]$, and $N[NO_2]$, $N[N_2O_5]$ are negligible. Active species N_{ac} must be present during daytime down to ~40 km [*Jursa*, 1985, p. 21–41], increasing the detachment coefficient from its photodetachment value of $\gamma_e = 0.44$ s^{-1} [*Gurevich*, 1978, p. 114] to ~1–15 s^{-1}. However, using this value produces an "overshoot" at intermediate times 10 s < t < 10 min, which is absent in data (see Figure 5). Best fits for amplitude during these times occur for $N_{ac} = 0$ (or
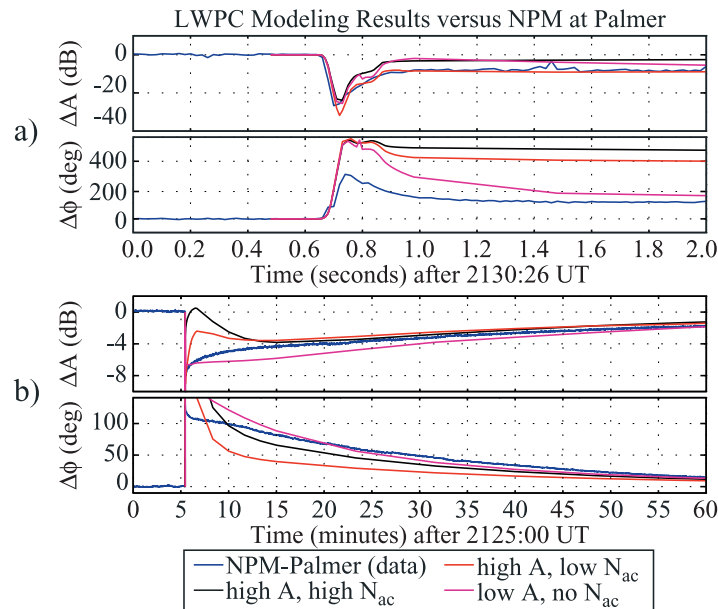
Figure 5. Results of calculations of VLF propagation along the NLM-PA path illuminated by γ-ray flare: (a) 2 s after the spike; (b) hour-long recovery, for 3 cases; with high A, with high A and N_{ac} reduced by a factor of 0.3, and with low A and $N_{ac} = 0$ (see text).
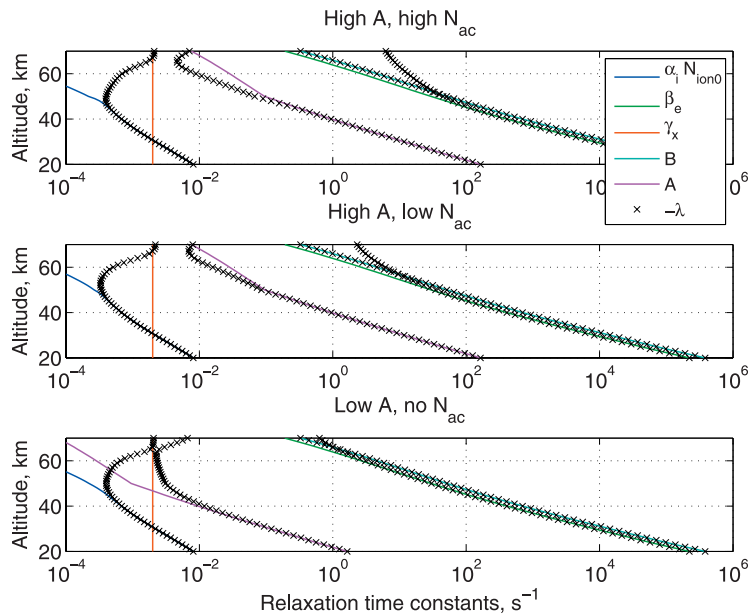
Figure 6. Time scales of 5-constituent model, for 3 cases of Figure 5; black crosses are time constants of linearized equations (1)−(5).

$N_{ac} \lesssim 10^9$ cm^{-3}, lower than the tabulated daytime value of $N[O] \gtrsim 10^{10}$ cm^{-3} [*Jursa*, 1985 p. 21−43]), which may be due to ambient conditions at the time of flare onset. High value of A reproduces observed VLF amplitude, but not the phase. Best results at all times are achieved with the "low" value of A and $N_{ac} = 0$, except for magnitude of the phase change for $t < 2$ s, overestimated by a factor of ~ 2. The remaining differences between model and data might be due to deficiencies in either the ionospheric relaxation model or the VLF propagation model or both.

[17] Time constants (absolute values of eigenvalues) of linearized equations (1)−(5) at subionospheric altitudes ($\lesssim 70$ km) and their relation to the ambient densities and coefficients are plotted in Figure 6, for values of A and N_{ac} used in Figure 5. The long time scale is due to ions and the rate of mutual neutralization (α_i). Other time scales are due to electron attachment rate (β_e) and rates of conversion of ions from one kind to another (A, B). All model curves give approximately correct time scale for the "slow" amplitude recovery, largely due to mutual ion neutralization rate. However, different models suggest different "intermediate" phase relaxation scales (the second smallest time constant), due to variation of A, as seen from Figure 6. The "overshoot" in the amplitude has the same time scale as the phase variation, probably because both are due to change in ionospheric reflection height.

4. Summary

[18] Analysis of the impact of the 27 December 2004 giant γ-ray flare from SGR 1806−20 on the dayside ionosphere indicates that: (1) ionization change was caused by initial flare peak, not by oscillating tail or afterglow; (2) mutual ion neutralization rate determines the long-enduring (1-hour) recovery of the enhanced ionization; (3) nature of brief 3 to 6 kHz emission is not yet clear, but may be due to a partially-coherent electromagnetic pulse

(EMP) caused by the γ-ray flare [*Karzas and Latter*, 1965]. The analysis of flare impact and resulting ionization used here is similar to that used for a previous nighttime event studied by *Inan et al.* [1999], except the new 5-constituent model of ionosphere relaxation [*Lehtinen and Inan*, 2007] for better description of low altitudes (<50 km).

References

Allcock, G. M., C. K. Branigan, J. C. Mountjoy, and R. A. Helliwell (1963), Whistler and other very low frequency phenomena associated with the high-altitude nuclear explosion on July 9, 1962, *J. Geophys. Res.*, *68*, 735−739.

Cheng, Z., and S. A. Cummer (2005), Broadband VLF measurements of lightning-induced ionospheric perturbations, *Geophys. Res. Lett.*, *32*, L08804, doi:10.1029/2004GL022187.

Cummer, S. A., T. F. Bell, U. S. Inan, and D. L. Chenette (1997), VLF remote sensing of high energy auroral particle precipitation, *J. Geophys. Res*, *102*, 7477−7484.

Fehsenfeld, F. C., and E. E. Ferguson (1974), Laboratory studies of negative ion reactions with atmospheric trace constituents, *J. Chem. Phys.*, *61*(8), 3181−3193, doi:10.1063/1.1682474.

Ferguson, E. E. (1979), Ion chemistry of the middle atmosphere, *NASA Conf. Publ.*, CP-2090, 71−88.

Fishman, G. J., and U. S. Inan (1988), Observation of an ionospheric disturbance caused by a gamma-ray burst, *Nature*, *331*, 418−420.

Glukhov, V. S., V. P. Pasko, and U. S. Inan (1992), Relaxation or transient lower ionospheric disturbances caused by lightning-whistler-induced electron precipitation bursts, *J. Geophys. Res.*, *97*, 16,971−16,979.

Gurevich, A. V. (1978), *Nonlinear Phenomena in the Ionosphere*, Springer, New York.

Haldoupis, C., T. Neubert, U. S. Inan, A. Mika, T. H. Allin, and R. A. Marshall (2004), Subionospheric early VLF signal perturbations observed in one-to-one association with sprites, *J. Geophys. Res.*, *109*, A10303, doi:10.1029/2004JA010651.

Hurley, K., et al. (2005), An exceptionally bright flare from SGR 1806−20 and the origins of short-duration γ-ray bursts, *Nature*, *434*, 1098−1103.

Inan, U. S., and D. L. Carpenter (1987), Lightning-induced electron precipitation events observed at L ~ 2.4 as phase and amplitude perturbations on subionospheric VLF signals, *J. Geophys. Res.*, *92*, 3293−3303.

Inan, U. S., A. Slingeland, V. P. Pasko, and J. V. Rodriguez (1996), VLF and LF signatures of mesospheric/lower ionospheric response to lightning discharges, *J. Geophys. Res.*, *101*, 5219–5238.

Inan, U. S., N. G. Lehtinen, S. J. Lev-Tov, M. P. Johnson, T. F. Bell, and K. Hurley (1999), Ionization of the lower ionosphere by γ-rays from a magnetar: Detection of a low energy (3–10 keV) component, *Geophys. Res. Lett.*, *26*, 3357–3360.

Jursa, A. S., (Ed.) (1985), *Handbook of Geophysics and the Space Environment*, Air Force Geophys. Lab., Springfield, Va.

Karzas, W. J., and R. Latter (1962), The electromagnetic signal due to the interaction of nuclear explosions with the Earth's magnetic field, *J. Geophys. Res.*, *67*, 4635–4640.

Karzas, W. J., and R. Latter (1965), Detection of the electromagnetic radiation from nuclear explosions in space, *Phys. Rev.*, *137*(5B), B1369–B1378, doi:10.1103/PhysRev.137.B1369.

Lehtinen, N. G., and U. S. Inan (2007), Possible persistent ionization caused by giant blue jets, *Geophys. Res. Lett.*, doi:10.1029/2006GL029051, in press.

Lev-Tov, S. J., U. S. Inan, A. J. Smith, and M. A. Clilverd (1996), Characteristics of localized ionospheric disturbances inferred from VLF measurements at two closely spaced receivers, *J. Geophys. Res.*, *101*, 15,737–15,747.

Mereghetti, S., D. Götz, A. von Kienlin, A. Rau, G. Lichti, G. Weidenspointner, and P. Jean (2005), The first giant flare from SGR 1806–20: Observations using the anticoincidence shield of the spectrometer on INTEGRAL, *Astrophys. J.*, *624*, L105–L108, doi:10.1086/430669.

Mitra, A. P. (1974), *Ionospheric Effects of Solar Flares*, Springer, New York.

Moore, R. C., C. P. Barrington-Leigh, U. S. Inan, and T. F. Bell (2003), Early/fast VLF events produced by electron density changes associated with sprite halos, *J. Geophys. Res.*, *108*(A10), 1363, doi:10.1029/2002JA009816.

Potemra, T. A., and T. J. Rosenbert (1973), VLF propagation disturbances and electron precipitation at mid-latitudes, *J. Geophys. Res.*, *78*, 1572–1580.

Terasawa, T., et al. (2005), Repeated injections of energy in the first 600 ms of the giant flare of SGR 1806-20, *Nature*, *434*, 1110–1111.

_____

S. Boggs and K. Hurley, Space Sciences Laboratory, University of California, Berkeley, 7 Gauss Way, Berkeley, CA 94708, USA.

G. J. Fishman, NASA Marshall Space Flight Center, Huntsville, AL 35812, USA.

U. S. Inan, N. G. Lehtinen, and R. C. Moore, STAR Laboratory, Stanford University, 350 Serra Mall, Stanford, CA 94305, USA. (nleht@stanford.edu)

D. M. Smith, Department of Physics, University of California, Santa Cruz, 1156 High Street, Santa Cruz, CA 95064, USA.